



High Thermoelectric Performance and Flexibility in Rationally Treated PEDOT:PSS Fiber Bundles

Ting Wu¹ · Xiao-Lei Shi² · Wei-Di Liu³ · Meng Li² · Fang Yue⁴ · Pei Huang¹ · Qingfeng Liu¹ · Zhi-Gang Chen² 

Received: 2 November 2023 / Accepted: 1 January 2024 / Published online: 27 February 2024
© The Author(s) 2024

Abstract

Organic thermoelectric fibers have great potential as wearable thermoelectric textiles because of their one-dimensional structure and high flexibility. However, the insufficient thermoelectric performance, high fabrication cost, and mechanical fragility of most organic thermoelectric fibers significantly limit their practical applications. Here, we employ a rapid and cost-effective wet-spinning method to prepare dimethyl sulfoxide-doped poly(3,4-ethylenedioxythiophene):poly(styrene sulfonate) (PEDOT:PSS) fiber bundles, followed by rational post-treatment with concentrated sulfuric acid (98% H₂SO₄) to enhance their thermoelectric performance. The wearable fiber bundles composed of multiple individual PEDOT:PSS fibers have effectively reduced resistance and overall high tensile strength and stability. Rational treatment with H₂SO₄ partially removes excessive PSS, thereby increasing the electrical conductivity to 4464 S cm⁻¹, while the parallel bundle is also a major factor in improving the power factor of up to 80.8 μW m⁻¹ K⁻², which is super-competitive compared with those of currently published studies. Besides, the thermoelectric device based on these fiber bundles exhibits high flexibility and promising output power of 2.25 nW at a temperature difference of 25 K. Our work provides insights into the fabrication of all-organic flexible high-conductivity textiles with high thermoelectric properties.

Keywords Thermoelectric · PEDOT:PSS · Fiber · Flexible device

Introduction

Electronic devices have gradually developed towards miniaturization and integration, bringing new opportunities for the development of implantable and wearable electronics [1].

However, the application of traditional batteries in wearable and implantable electronic products is necessarily limited because they require frequent replacement, charging, and additional maintenance [1]. Therefore, the development of maintenance-free and self-powered power sources is of great significance for the next generation of wearable and implantable electronics. Thermoelectric materials, which directly convert heat from the surrounding environment into electricity via the thermoelectric effect without polluting the environment, have become one of the most competitive candidate materials for environmentally friendly energy conversion [2]. The dimensionless figure-of-merit, $ZT = S^2\sigma T/\kappa$, is mainly used to evaluate the thermoelectric potential of a material, which is composed of the Seebeck coefficient S , the electrical conductivity σ , the absolute temperature T , and the thermal conductivity κ [3]. However, traditional bulk thermoelectric materials have many drawbacks including complex processing, large and rigid volumes, and high cost, making them unsuitable for wearable devices [4]. In this regard, flexible thermoelectric materials exhibit significant advantages since they can effectively contact and collect heat from bent heat sources [4]. Compared to other rigid devices,

Ting Wu and Xiao-Lei Shi contributed equally to the work.

✉ Qingfeng Liu
qfliu@njtech.edu.cn

✉ Zhi-Gang Chen
zhigang.chen@qut.edu.au

- ¹ State Key Laboratory of Materials Oriented Chemistry Engineering, College of Chemistry Engineering, Nanjing Tech University, Nanjing 211800, Jiangsu, China
- ² School of Chemistry and Physics, ARC Research Hub in Zero-Emission Power Generation for Carbon Neutrality, Centre for Materials Science, Queensland University of Technology, Brisbane, QLD 4000, Australia
- ³ Australian Institute for Bioengineering and Nanotechnology, The University of Queensland, Brisbane, QLD 4072, Australia
- ⁴ Merino & Co Ltd, Osborne Park, WA 6017, Australia

flexible thermoelectric devices (FTEDs) are lighter in weight and can be comfortably attached to human skin to directly collect electrical energy from body heat without the need for charging, and they can also prevent or minimize heat loss during energy transfer [1]. These advantages make them a promising contender for one of the most competitive power supply systems for wearable electronic devices [1].

Inorganic thin films [5], conducting polymers [6], and their composites [7] are the main candidates for fabricating FTEDs. Among them, inorganic thin films usually exhibit high thermoelectric performance, but their flexibility is poor [7]. Conducting polymers and inorganic/organic composites possess much better flexibility, but their thermoelectric properties need to be improved due to their poor S [7]. As a promising conductive polymer, poly(3,4-ethylenedioxythiophene):poly(styrene sulfonate) (PEDOT:PSS) is a highly valuable flexible material because of its unique characteristics including high σ , low κ , low cost, and facile preparation [6], which enables PEDOT:PSS having wide application prospects in flexible electronics, energy conversion, and thermal management. Moreover, it is easy to tune the electrical and thermal properties of PEDOT:PSS by controlling its chemical structure and physical morphology. Historically, there are mainly four routes used to improve the thermoelectric performance of PEDOT:PSS, including (1) doping conductive fillers (such as metals [8], and carbon nanotubes [9]) into PEDOT:PSS to increase the σ , but the κ may be simultaneously increased, (2) changing the post-treatment conditions of PEDOT:PSS (such as solvent [10], concentration [11], temperature [12]), by which the crystal structure of PEDOT:PSS can be controlled to adjust the electrical and thermal properties, (3) introducing chemical modification groups (such as hydrophilic/hydrophobic groups [13, 14], and surfactant [15]) to change the molecular structure and surface properties of PEDOT:PSS, and (4) controlling the molecular weight of PEDOT:PSS to adjust the electrical and thermal properties via rational treatments [6]. Other methods such as controlling the oxidation level of PEDOT electrochemically were also employed to improve the thermoelectric properties of PEDOT:PSS [16, 17].

Compared with two-dimensional (2D) PEDOT:PSS films, one-dimensional (1D) PEDOT:PSS thermoelectric fibers have stronger structural design flexibility in practical applications, and their ease of bending and weaving make them more suitable for wearable thermoelectric devices (TEDs) [18]. Therefore, the development of highly thermoelectric and ultra-flexible fibers is of significance for the rapid development of wearable electronic devices [19]. Currently, pre- and post-treatments and hybridizations, developed in 2D PEDOT:PSS films [20], are used to prepare 1D PEDOT:PSS thermoelectric fibers. However, there are still many issues in PEDOT:PSS fibers for practical applications. For example, the poor controllability of

PEDOT:PSS thermoelectric fibers easily induces fiber fracture or excessive structural modification during pre- and post-treatments, leading to significantly reduced thermoelectric performance. Moreover, the mechanical properties of thermoelectric fibers are poorer than those of 2D films, which seriously affects their flexibility, wearability, and performance stability. Therefore, exploring new design routes is urgent for the development of PEDOT:PSS thermoelectric fibers with high tensile strength and thermoelectric performance.

Historically, most studies on PEDOT:PSS thermoelectric fibers mainly focus on single fibers, and the conductivity improvement of a single fiber is limited [21, 22] and this is one of the reasons that cause the above issues including the difficulty in concisely controlling the treatments and the low mechanical properties. The PEDOT:PSS fibers are combined with carbon nanotube [23] or tellurium nanowires [8]; the thermoelectric properties of the fibers after acid or alkali treatment are improved, but the subsequent two-step treatment process is complex and the economic cost of additives is increased. The introduction of tellurium nanowires increased the Seebeck coefficient while reducing the rheological properties of the fibers. In fact, compared with individual PEDOT:PSS thermoelectric fibers, fiber bundles composed of multi-fibers exhibit better performance due to their higher strength, stiffness, and toughness, which enable them to withstand greater stress, better maintain shape and structure, and reduce the risk of damage during use. The innovation in this work lies in the optimization of the traditional wet-spinning process, producing thermoelectric fiber bundles composed of multiple fibers. The unique feature is that the conductivity of the fiber bundle is enhanced without any post-treatment, thanks to the aggregation of fibers. The increased diameter of the fiber bundle improves the tensile strength of the fibers, enhancing their resistance to deformation in practical applications. Because, fiber bundles have a more flexible surface area and a certain depth, allowing them to provide positive feedback on pre- and/or post-treatments without compromising their structures and resulting in greater flexibility. Based on this concept, we employ a rapid wet-spinning method to prepare dimethyl sulfoxide (DMSO)-doped PEDOT:PSS fibers (DPFs) and combine the as-achieved fibers into fiber bundles, followed by rational post-treatment with concentrated sulfuric acid (98% H_2SO_4) to further enhance the thermoelectric performance of the fiber bundles, as illustrated by Fig. 1a. DMSO addition could help to improve the fiber spinnability [24] and hydrogen bonding between PSSH and DMSO is the dominant interaction in DMSO-treated PEDOT:PSS, which causes to charge screening and phase separation of PEDOT:PSS [25]. After forming hydrogen bonds with PSS, dipole–dipole or dipole–charge interactions can occur [26]. Therefore, electrical conductivity can be improved and

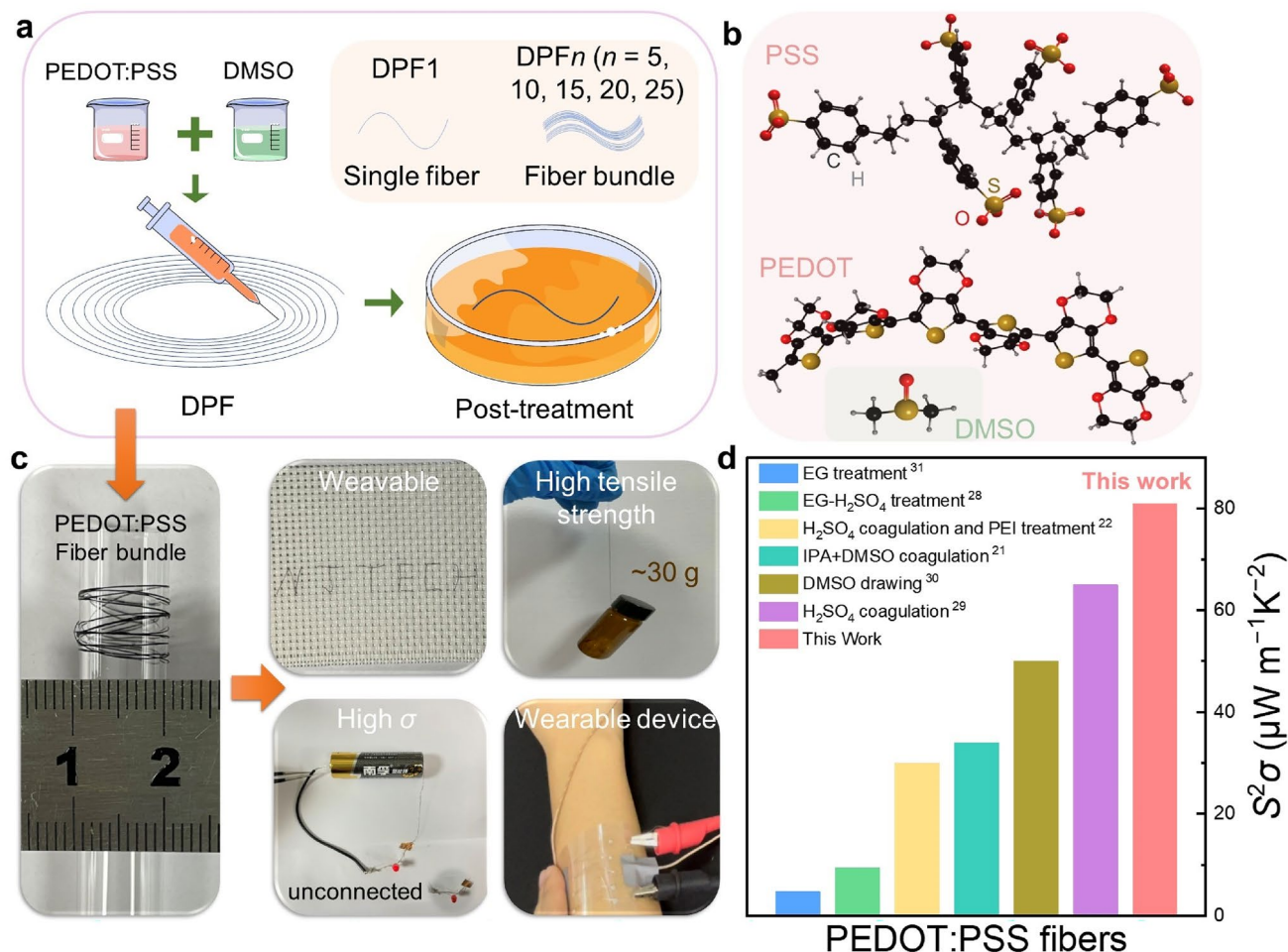


Fig. 1 Introduction of PEDOT:PSS thermoelectric fiber bundle and their performance. **a** Illustration of fabricating dimethyl sulfoxide (DMSO)-doped poly(3,4-ethylenedioxythiophene):poly(styrene sulfonate) (PEDOT:PSS) fiber (DPF) bundles by wet-spinning, followed by rational post-treatment with concentrated sulfuric acid (98%

H₂SO₄). **b** Structures of PEDOT, PSS, and DMSO. **c** Photographs of as-fabricated PEDOT:PSS fiber bundles and their wearable, highly tensile strength, electrically conductive, and wearable features. **d** The room-temperature power factor $S^2\sigma$ of this work and reported works based on pure PEDOT:PSS fibers [21, 22, 28–31]

DMSO is a good additive for PEDOT:PSS for wet spinning. Here, the fiber bundles are defined as DPF n , where n is the number of individual fibers in a bundle (for example, DPF10 indicates a fiber bundle composed of 10 individual fibers). We obtained different fiber bundles by controlling the rotation of the coagulation bath (see Supporting video). When the coagulation bath is rotating uniformly in a circular motion, the needle is stationary at 6 cm from the center of the circumference. When the coagulation bath rotates 360° with respect to the needle, the collected fiber is DPF1; similarly, repeated rotation for n 360° is defined as DPF n . Figure 1b shows the molecular structures of PEDOT, PSS, and DMSO. As DMSO is a polar solvent, DMSO pre-treatment can reduce the charge inhibition effect of PSS in PEDOT:PSS, leading to enlarged σ [27]. At the same time, DMSO can promote the formation and growth of PEDOT:PSS crystals, thereby enhancing their crystalline

quality and thermoelectric properties [27]. Besides, H₂SO₄ post-treatment on PEDOT:PSS fiber bundles can partially remove excessive PSS molecules from PEDOT:PSS, leading to an increase in the σ [27]. Finally, considering the certain depth of the bundles, H₂SO₄ post-treatment does not damage the structure of PEDOT:PSS. Figure 1c shows the typical photographs of the as-fabricated PEDOT:PSS fiber bundles and their engineering, which exhibit wearable, tensile strength, electrically conductive, and wearable features. The as-fabricated bundles can withstand the weight of heavy objects without breaking. Additionally, the bundles have good knitting ability and can adhere well to fabrics. Moreover, the bundles treated with H₂SO₄ can act as conductors to light-emitting diodes (LEDs) in a circuit with batteries. Figure 1d compares the room-temperature power factor $S^2\sigma$ of this work with the reported works based on pure PEDOT:PSS fibers (detailed parameters are summarized in

Table S1 in the Supporting Information) [21, 22, 28–31]. The as-achieved $S^2\sigma$ of $> 80 \mu\text{W m}^{-1} \text{K}^{-2}$ is highly competitive compared with those of the previously published works. Furthermore, we fabricated the fiber bundles into FTEDs to measure their applicability, and the results indicate the potential for charging low-grade wearable electronics.

Experiment Sections

Chemicals

The poly (3,4-ethylenedioxythiophene):poly (styrene sulfonate) (PEDOT:PSS) aqueous dispersion (Clevios PH1000) was purchased from Heraeus. Dimethyl sulfoxide (DMSO, AR) was purchased from Shanghai Macklin Biochemical Co., Ltd. Isopropanol (IPA, AR, 99.7%) and ethanol absolute were purchased from Sinopharm Chemical Reagent Co., Ltd. Ethylene glycol (EG, AR, 99%) and sulfuric acid (H_2SO_4 , AR, 98%) were purchased from Shanghai LingFeng Chemical Reagent Co., Ltd. Formamide (CH_3NO , AR, 99%) was purchased from Shanghai Aladdin Biochemical Technology Co., Ltd. The deionized water is made by the Laboratory Water Purification System from Hitech Instruments Co., Ltd.

Wet-Spinning of Dimethyl Sulfoxide (DMSO)-Doped PEDOT:PSS Fiber Bundles

The spinning solution was prepared by heating the PEDOT:PSS (1 ml) containing 5 wt% DMSO at 90°C for 2 h with stirring. The spinning solution was then kept at 0°C for 24 h to increase the viscosity. DMSO-doped PEDOT:PSS single fiber and fiber bundles were prepared at room temperature using a micro syringe pump device from Badding Longer Precision Pump Co., Ltd. A 3 ml syringe and a 25 G needle were used for the wet-spinning procedure. Isopropyl alcohol on the rotary table was used as a coagulation bath. The wet-spinning rate was controlled at $50 \mu\text{l min}^{-1}$. When the needle rotates one turn relative to the IPA coagulation bath, paused the syringe pump. The sample collected at this moment is a single fiber named DPF1. Similarly, when the syringe pump was paused after 5, 10, 15, 20, and 25 consecutive rotations, the collected samples were fiber bundles consisting of 5, 10, 15, 20, and 25 single fibers. The process of wet-spun DPF10 is shown in the supporting video. These samples were named DPF5, DPF10, DPF15, DPF20, DPF25, respectively. All the samples collected from the IPA coagulation bath were rinsed with ethanol and then dried on a heating plate at 60°C for 10 min. All the samples were collected from the IPA coagulation bath and then rinsed with

a mixture of ethanol absolute and deionized water (3:1 v/v) and then dried on a heating plate at 60°C for 10 min.

Post-Treatment of Dimethyl Sulfoxide (DMSO)-Doped PEDOT:PSS Fiber Bundles

The dried DPF1 was immersed in EG, DMSO, CH_3NO , and H_2SO_4 for 120 min, respectively. The post-treated samples were repeatedly rinsed with a mixture of ethanol and deionized water (3:1 v/v) and then dried on a heating plate at 90°C for 15 min. For the concentrated sulfuric acid post-treatment process of fiber bundles, DPF5, DPF10, DPF15, DPF20, and DPF25 were immersed into 98% H_2SO_4 and left to stand for 1, 5, 10, 30, 60, and 120 min, respectively. Similarly, the soaked fiber bundle samples were repeatedly rinsed with a mixture of ethanol and deionized water (3:1 v/v) and then dried on a heating plate at 90°C for 15 min.

Characterization and Thermoelectric Property Measurement

The surface morphology and cross-sectional morphologies of the single fiber and fiber bundles were conducted on scanning electron microscopy (SEM, S-4800). The oxidation levels of the samples were characterized by X-ray photoelectron spectroscopy (XPS, Thermo ESCALAB 250, country). Raman spectroscopy was performed from 1200 to 1800 cm^{-1} on a confocal Raman microscope (LabRAM HR Evolution) using a 553 nm laser. The mechanical testing was conducted with a homemade tensile Testing Machine at a strain rate of 0.2 mm min^{-1} . A four-probe test sample was prepared by taking a 5 cm length of DPF10 with H_2SO_4 post-treated on a polyvinyl chloride (PVC) film. The bending durability test was conducted at different diameters and held for at least 1 day and then measured the S and R .

The S of the samples was measured at room temperature with PTM-3 from WuHan Jouleyacht Science & Technology Co., Ltd. The σ were measured using a homemade four-probe method. The electrical resistance R was determined by a classical 4-probe in-line contact method with a Keithley 2450 source/meter. The diameter of the samples was measured by metallographic microscopy (CX40M) from Ningbo Shunyu Instrument Co., Ltd. The σ was calculated using Eq. (1);

$$\sigma = L/AR, \quad (1)$$

where R (Ω) is the electrical resistance, A (cm^2) is the cross-sectional area, and L (cm) is the distance between electrodes. For all samples, their diameters, R , and σ values were averaged by measuring at least five times. For a single fiber, the cross-sectional area of DPF1 is calculated from the diameter measured by metallographic microscopy, according to Eq. (2);

$$A = \pi D^2 / 4, \quad (2)$$

where D (μm) is the diameter of a single fiber. For fiber bundles, the cross-sectional area of the fiber bundles is calculated to be equivalent to the area of a rectangle, according to Eq. (3);

$$A = 2D \times D \text{ or } A = 3D \times D. \quad (3)$$

The length of the cross-sectional area was the data measured by metallographic microscopy D' (μm); the width was twice the diameter of the single fibers (2D) for DPF1 and DPF5 and three times the diameter of the single fibers (3D) for DPF10, DPF15, and DPF25. The error bars in the figure originate from the standard variance calculated based on multiple measurement values.

Device Fabrication and Performance Evaluation

Thermoelectric devices were prepared from five fiber bundles of 2.5 cm in length and were neatly arranged on a PVC film and the fiber bundles were connected using a highly conductive silver paste. Two copper leads are connected at the ends of the device with conductive copper tape for testing. When the device used the human arm as the heat source, the open circuit voltage was tested by a Keithley DAQ6510 multimeter. In the case of using a heating plate as a heat source, the other end was exposed to air to obtain a higher thermal voltage by increasing the temperature of the heating plate. The maximum output power P of the device was obtained by adjusting the constant value resistor in the circuit. We have obtained full consent from human research participants in this work for wearable devices.

Results and Discussion

Thermoelectric Performance of PEDOT:PSS Fiber

We first evaluated the room-temperature thermoelectric performance of PEDOT:PSS fiber bundles, including DPF n ($n = 1, 5, 10, 15, 20,$ and 25). Figure 2a compares the σ , S , and $S^2\sigma$ of DPF n ($n = 1, 5, 10, 15, 20,$ and 25) without any post-treatment. With increasing the number of individual fibers n in the fiber bundle, the σ shows an initially increasing trend followed by a decreasing trend. The best performance for the thermoelectric fiber bundle can be achieved when the bundle consists of 10 individual fibers, which exhibits a significantly higher σ compared to other bundles. When n is 10, the intensity of interfaces between individual fibers is an optimized value for electrical transport; however, when n is > 10 , the reason for the drop of σ is that the increased number of fibers leads to loosen bonding between the fibers and the appearance of gaps that increase interfacial resistance.

Another reason could be that the isopropanol used to coagulate the fibers may hinder charge carrier transport by being trapped within the fiber bundle. Besides, with increasing the n , the S is almost the same value, this is because the S is not sensitive to the structures (interfaces) but the composition, which further explains the phenomenon discussed above.

To improve the thermoelectric performance of DPF, we tested different post-treatment methods, including EG, DMSO, CH_3NO , and H_2SO_4 for 120 min. The results indicate that the DPF post-treated with H_2SO_4 possesses the highest thermoelectric performance (Fig. S1), which should be attributed to that H_2SO_4 is the most effective post-treatment method to remove the excessive PSS, confirmed by the Raman spectrum and high-resolution X-ray photoelectron spectroscopy (XPS) results (Fig. S2). After H_2SO_4 treatment, a portion of the PSS ions is neutralized by the protons from H_2SO_4 , leading to the disappearance of the Coulombic attraction between PEDOT and PSS. This results in the substitution of the PSS unit by the hydrogen sulfate ion as the counterion for the PEDOT particle. The deconvolution of the S2p spectra for DPF treated with H_2SO_4 for 120 min (Fig. S2c) reveals that the binding energies at 164.1–165.2 eV and 167.2–168.3 eV are attributed to sulfur in the thiophene ring and PSS, respectively. The peak at the binding energy of 169.5–170.4 eV corresponds to sulfate, indicating the successful substitution of bisulfate for PSS in PEDOT. Based on these results, we choose H_2SO_4 to post-treat the as-achieved bundles and explore the suitable treatment time. Figure 2b shows the σ , S , and $S^2\sigma$ of DPF10 post-treated by 98% H_2SO_4 at different treating times. As can be seen, 120 min treatment can induce the highest σ and in turn the highest $S^2\sigma$. This is because a longer treatment time can remove too much PSS, leading to damaged DPF10. On this basis, 120 min should reach the upper limit. Figure 2c plots the σ , S , and $S^2\sigma$ of DPF n post-treated by 98% H_2SO_4 with a treatment time of 120 min. As can be seen, when $n = 10$, a peak σ of $\sim 4464 \text{ S cm}^{-1}$ can be seen, leading to an optimized $S^2\sigma$ of $80.8 \mu\text{W m}^{-1} \text{ K}^{-2}$. Such a phenomenon is also derived from the optimized interface intensity. Figure 2d compares the σ between our study and the reported in PEDOT:PSS-based fibers [8, 9, 21–24, 28–53]. As can be seen, our as-achieved σ is the highest. More detailed parameters are summarized in Table S2 in the Supporting Information for reference.

Morphology and Structure Characterization of PEDOT:PSS Fiber

To understand the as-achieved high thermoelectric properties in our PEDOT:PSS fiber bundles, we investigated comprehensive structural and morphological characterizations. Figure 3a–c shows SEM images of DPF1 (single fiber), DPF10, and DPF25, which are all without post-treatment.

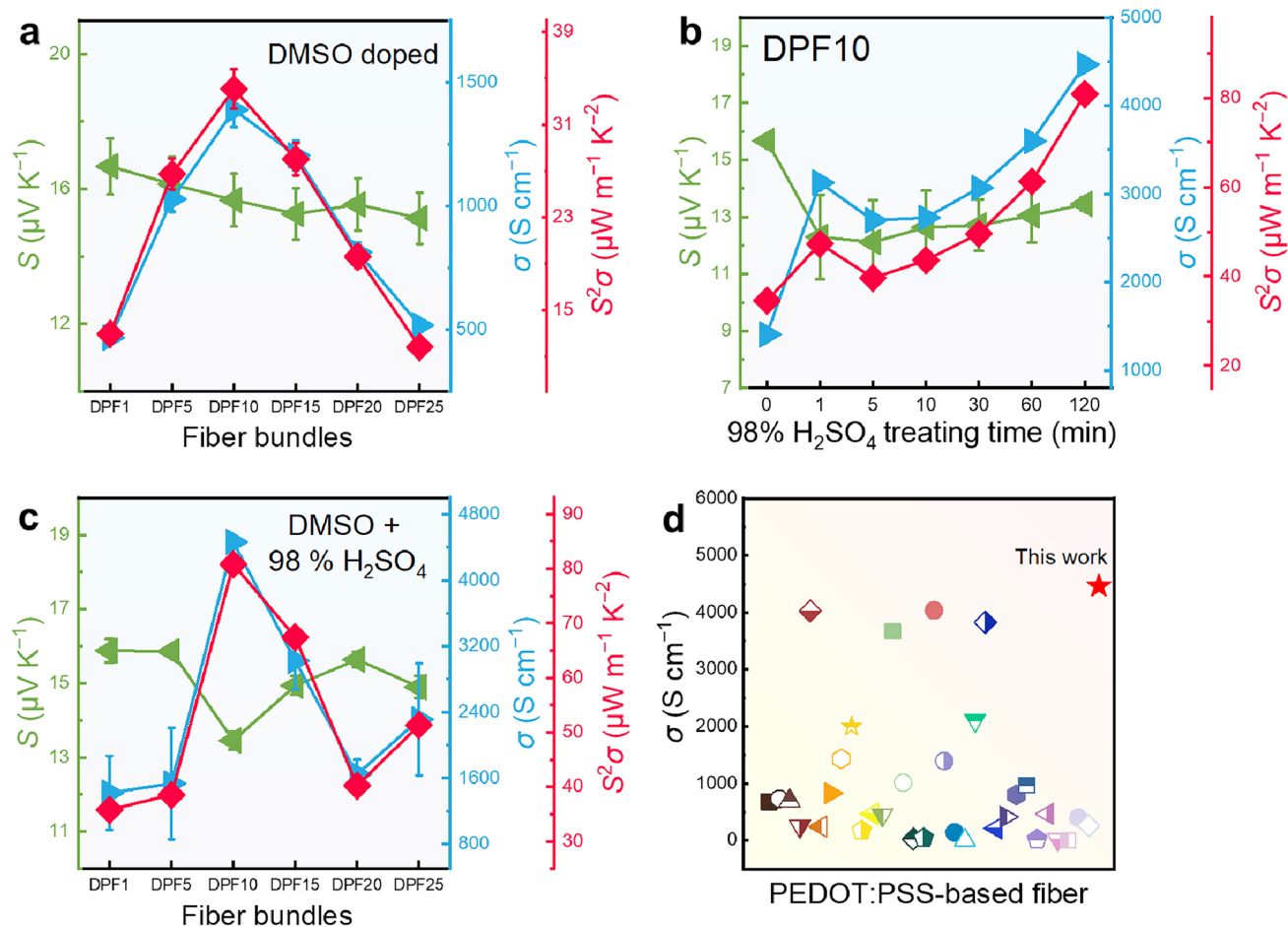


Fig. 2 Room-temperature thermoelectric performance of PEDOT:PSS fiber bundles. **a** Electrical conductivity σ , Seebeck coefficient S , and $S^2\sigma$ of DPF n ($n=1, 5, 10, 15, 20$, and 25). Here, n indicates the number of individual fibers in one bundle. **b** σ , S , and $S^2\sigma$ of DPF10 post-treated by 98% H_2SO_4 with different time. **c** σ , S , and $S^2\sigma$ of DPF n post-treated by 98% H_2SO_4 with 120 min. **d** Comparison of σ between this work and reported works based on PEDOT:PSS-based fibers [8, 9, 21–24, 28–53]

As can be seen, when the number of individual fibers is small, PEDOT:PSS fibers form tightly packed fiber bundles in the solidification bath. However, when the fiber bundle has 10 fibers ($n > 10$), due to the rapid solidification of the fibers in the bath, the subsequent fibers are unable to bond tightly with the previous fibers, resulting in a less uniform fiber arrangement with gaps in the middle. The SEM images of DPF5, DPF15, and DPF20 are shown in Fig. S3 for reference. In addition to SEM results, Fig. 3d compares Raman spectra of DPF n ($n=1, 5, 10, 15, 20$, and 25). The main forces between PEDOT:PSS are electrostatic interactions and π - π stacking. PEDOT is responsible for conductivity, while PSS balances electrode polarity and facilitates the dissolution of PEDOT. The enhancement of the conductivity of PEDOT:PSS is primarily achieved by disrupting the electrostatic binding forces between PEDOT and PSS, thereby increasing the crystallinity of PEDOT itself. As the number of fiber bundles increases, the Raman characteristic peak width decreases at 1427 cm^{-1} , indicating an increase in

crystallinity [26]. Consequently, the fiber bundle resistance measured by the four-probe method decreases. The conductivity is calculated by considering the fiber resistance and the corresponding cross-sectional area. The cross-sectional area of the fiber bundle increases with the increasing number of fibers, leading to an initial rise and subsequent decrease in the overall conductivity (Fig. 2a). Figure 3e compares high-resolution XPS patterns of DPF n ($n=1, 5, 10, 20$, and 25) for S2p. No significant shifts or changes can be seen in both Raman and XPS, indicating that the formation of fiber bundles did not alter their molecular structure. It can be inferred that the enhancement of electrical performance in fiber bundles is due to physical changes (mainly interfaces). Figure 3f shows high-resolution S2p XPS patterns of DPF10 post-treated by 98% H_2SO_4 at different times. The peaks shifting toward lower binding energy indicates the effective removal of PSS parts. Figure 3g shows an SEM image of DPF1 post-treated by 98% H_2SO_4 . The diameter was reduced from 18.2 to 7.9 μm after 98% H_2SO_4

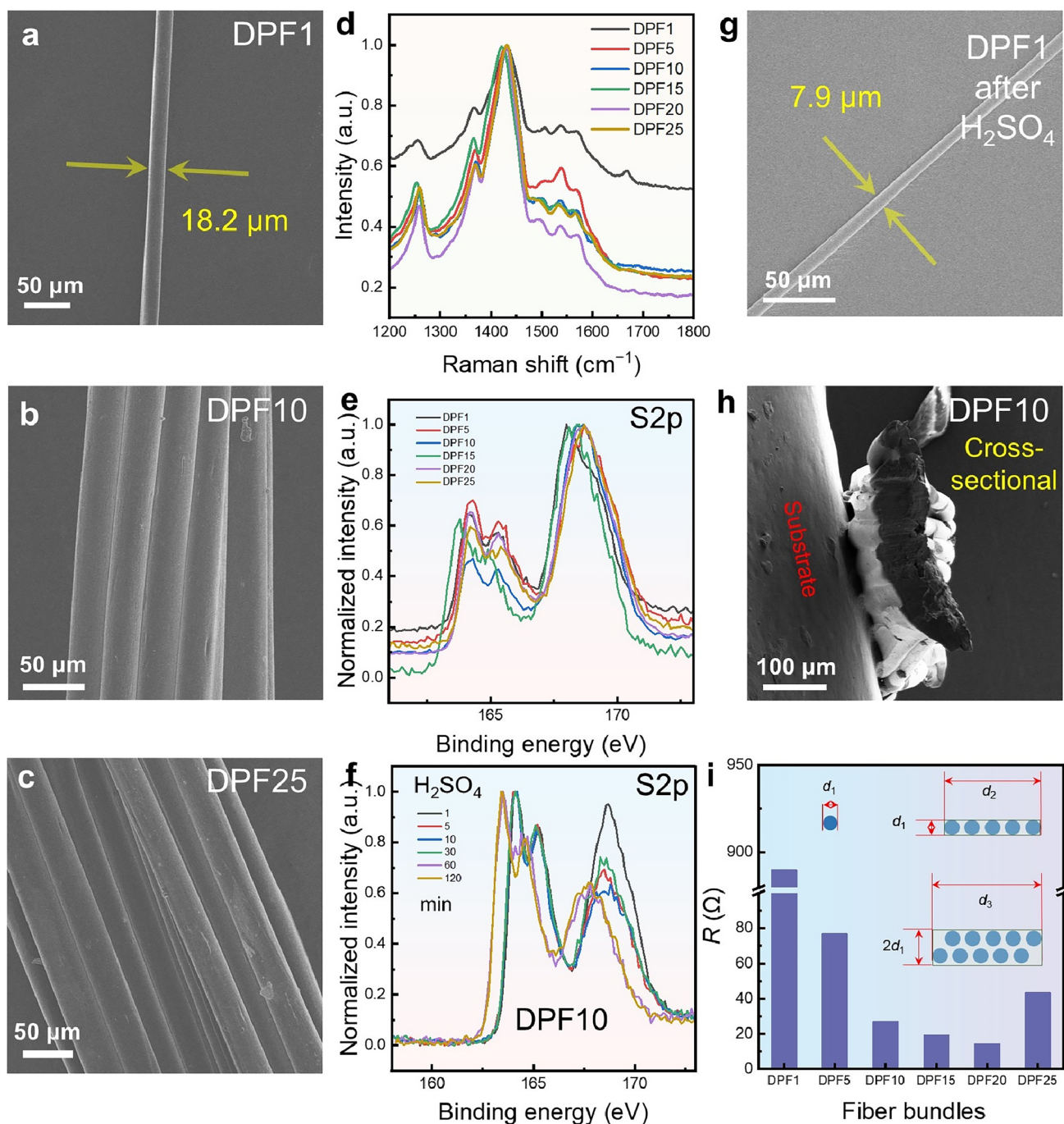


Fig. 3 Characterizations of PEDOT:PSS fiber bundles. Scanning electron microscopy (SEM) images of **a** DPF1, **b** DPF10, and **c** DPF25. **d** Raman spectra of DPF n ($n=1, 5, 10, 15, 20,$ and 25). **e** High-resolution X-ray photoelectron spectroscopy (XPS) patterns of DPF n ($n=1, 5, 10, 20,$ and 25) for S2p. **f** High-resolution XPS patterns of DPF10 post-treated by 98% H₂SO₄ with different treating

times for S2p. **g** SEM image of DPF1 post-treated by 98% H₂SO₄. **h** Cross-sectional SEM image of severed DPF10 by a scissor. **i** Measured resistance R of DPF n ($n=1, 5, 10, 15, 20,$ and 25). The inset shows the cross-sectional area of a fiber bundle that is used to calculate the conductivity

post-treatment, further confirming the partial removal of the excessive PSS. The metallographic microscope images of DPF n ($n=1, 5, 10, 15, 20,$ and 25) post-treated by 98% H₂SO₄ with 120 min are shown in Fig. S4 for reference.

Figure 3h shows a cross-sectional SEM image of severed DPF10 by a scissor. So the shape of the soft polymer was changed slightly. As can be seen, when there are many individual fibers in the bundle, fiber stackings occur instead of

all fibers arranged in a single layer. Also, there is no obvious boundary between individual fibers, indicating that the σ should be high due to the less carrier scattering. The cross-sectional SEM images of DPF5, DPF15, DPF20, and DPF25 can be referred to in Fig. S5, which further confirms this result. Based on this phenomenon, Fig. 3i shows the measured resistance R of DPF n ($n = 1, 5, 10, 15, 20,$ and 25). The inset shows the cross-sectional area of a fiber bundle that was used to calculate the σ . In the wet-spinning process, the needle diameter, injection rate, and rotation speed of the coagulation bath are consistent. Individual fibers are neatly aligned and undergo slight morphological changes in the coagulation bath due to factors such as the gravity of the fibers before solidification, resulting in a non-ideal cylindrical shape. We captured the surface morphology of individual fibers using SEM and found that each fiber is uniform with a cross-sectional circular shape. The measured length on the fiber surface corresponds to the cross-sectional diameter of the fiber. Fiber bundles are formed by the accumulation of individual fibers, thus reasonably deducing that the ideal cross-sectional model of a fiber bundle is an assembly of individual fibers. Due to experimental factors, fiber bundles do not exhibit an ideal arrangement of cylindrical shapes but rather form a surface with integrated fiber structures. As a result, the cross-section of the fiber bundle is a multiple of the uniform cross-sectional diameter of individual fibers. Here, we assume that each fiber can be treated as a resistor, and the fiber bundle can be regarded as a system of resistors in parallel. According to Ohm's Law, the more resistors in parallel, the lower the overall resistance of the system. With increasing the number of individual fibers in the bundle (n), the resistance of the fibers was rapidly decreased except for $n = 25$. The R of the fiber is calculated from the average of five measurements. Based on the resistance values and the method of calculating the cross-sectional area, we measured the σ of the fiber bundle using a homemade four-probe method, which is the original of the measured σ shown in Fig. 2.

In addition to the improved thermoelectric properties, PEDOT:PSS fiber bundles also exhibited much higher mechanical performance than individual fibers. Figure 4a shows a photograph of a knotted DPF10. During the knotting process, the fiber bundle is stable without damage, especially for the knotted area, as shown in the SEM image in Fig. 4b. Figure 4c shows the measured normalized Seebeck coefficient S/S_0 and resistance R/R_0 of DPF10 as functions of knot number. Obviously, with increasing the knot number, the S/S_0 is stable because the S is not sensitive to the structure, while the R/R_0 only slightly increases, indicating good stability and wearability. In addition to the knotting test, we also performed traditional flexibility and strain–stress tests. Figure 4d shows a photograph of the flexibility test of DPF10 with a radius of curvature of 12.5 mm, and Fig. 4e shows the

measured S/S_0 and R/R_0 of DPF10 as functions of bending radius. Obviously, with decreasing the bending radius, both the S/S_0 and R/R_0 maintain stability, indicating outstanding flexibility. We further measured the tensile strength of DPF n ($n = 1, 5, 10, 15, 20,$ and 25), and the results are shown in Fig. 4f. The test results show a nonlinear slope of the stress as a function of strain. For DPF10, the initial slope is large and gradually slows down. When the maximum stress is reached, the fiber bundle breaks completely. The fracture length of fiber bundles increases as n increases. This may be due to the relaxation of the fiber bundles in the test performance [54]. With increasing the n , the tensile strength significantly increases, indicating outstanding rigid and strong bearing capacity. These results indicate that the as-designed fiber bundles can be applied to scenarios of any shape, and their thermoelectric properties remain largely unchanged, making it convenient to further process fiber bundles into wearable and wearability devices.

Home-Made Thermoelectric Device of PEDOT:PSS Fiber Bundles

To evaluate the practical application potential of as-fabricated PEDOT:PSS fiber bundles, we fabricated FTEDs composed of these fiber bundles as thermoelectric elements. Figure 5a illustrates the structure of the as-designed FTEDs composed of five DPF10 as p-type legs and we connected the two ends for testing using copper wires and an electrical meter. Figure 5b shows its optical image, in which a PVC film acted as the substrate to support the fiber bundles and wires. Figure 5c shows the photo of the power output (P) evaluation of the FTED composed of DPF10 under a temperature difference ΔT of 2.1 K between the environment and the human arm. The maximum output power P_{\max} of the FTED was obtained by adjusting the constant value resistor in the circuit. In addition to the FTED composed of DPF10, we also fabricate FTEDs composed of DPF5, DPF15, DPF20, and DPF25, respectively, and their photographs are shown in Fig. S6 for reference. Figure 5d compares measured open-circuit voltage V and R of the FTEDs composed of DPF n ($n = 5, 10, 15, 20,$ and 25). With increasing the n , the R decreases while V increases. In terms of the FTED composed of PDF10, Fig. 5e, f shows measured V and P as a function of loading current I_{load} under different ΔT s (10 K and 25 K). With increasing the I_{load} , the V decreases, and the P peaks at $\sim 1.75 \mu\text{A}$. Besides, with increasing the ΔT , both the V and P increase. A high P of 2.25 nW was achieved when $\Delta T = 25$ K, indicating the potential of charging low-grade wearable electronics. Besides, with increasing n , the P increases, as indicated by Fig. S7 for reference.

The wearable TEDs prepared from fiber bundles are expected to play a significant role in energy harvesting and human health monitoring. This self-sustaining energy

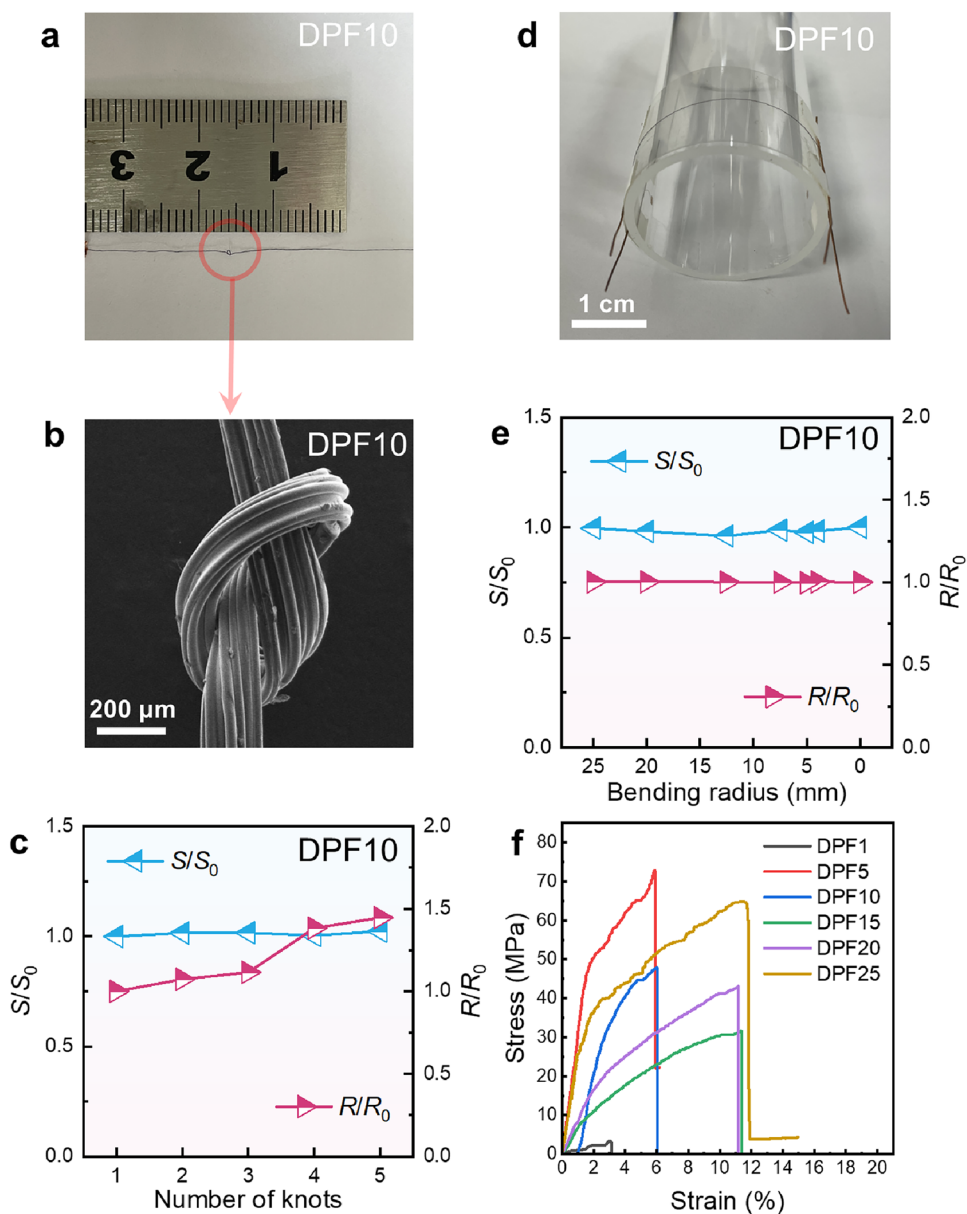


Fig. 4 Mechanical performance of PEDOT:PSS fiber bundles. **a** Photograph of a DPF10 bundle that can be knotted. **b** SEM image of the knot in **a**. **c** Measured normalized Seebeck coefficient S/S_0 and resistance R/R_0 of DPF10 as a function of knot number. **d** Photograph of the flexibility test of DPF10 with a radius of curvature of 12.5 mm. **e** Measured S/S_0 and R/R_0 of DPF10 as a function of bending radius. **f** Strain–stress curves of DPF n ($n = 1, 5, 10, 15, 20, \text{ and } 25$)

solution will reduce reliance on traditional batteries, driving the development of sustainable energy technologies. With advancements in nanotechnology and materials science, the performance of these TEDs is poised for significant improvement, making their applications in daily life and special environments more widespread and practical.

Additionally, these TEDs can be integrated with other smart materials and devices, such as optoelectronics for multifunctional capabilities like illumination and display. With the continuous progress of technology, we have reason to believe that these materials will play crucial roles in the future of smart textiles and energy technology.

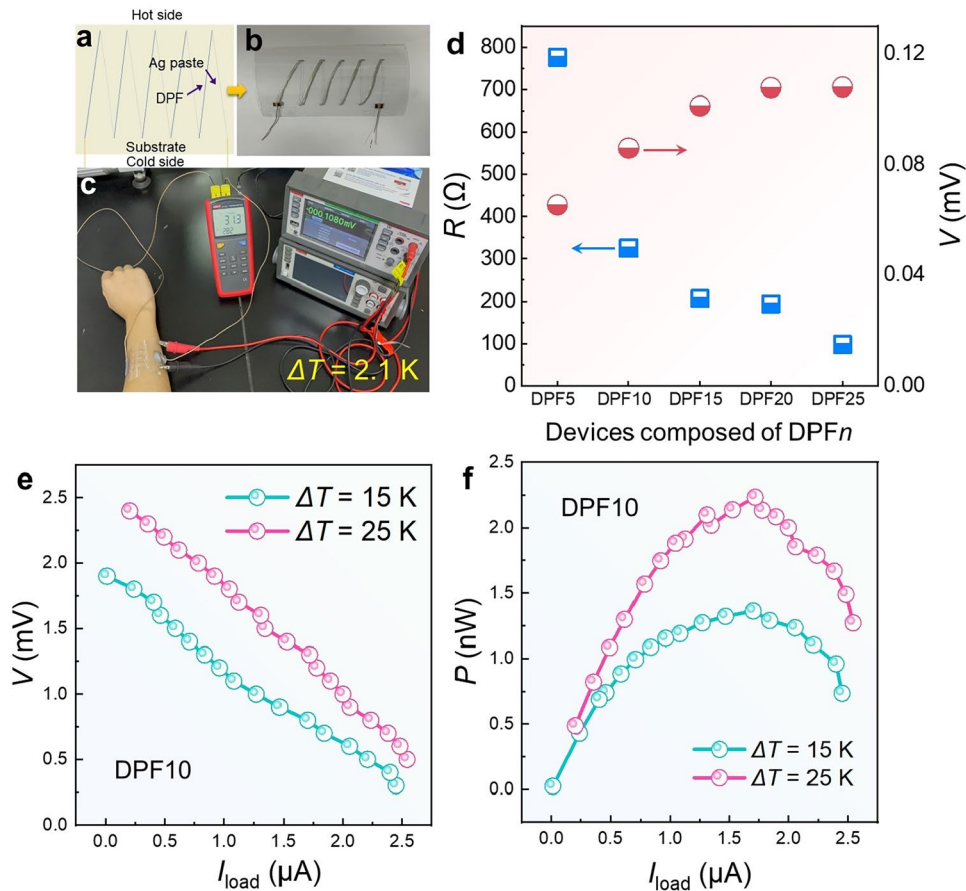


Fig. 5 Device performance based on PEDOT:PSS fiber bundles. **a** Illustrated structure and **b** photograph of the device composed of five DPF10 as p-type legs. **c** Photograph of the output evaluation of the wearable device under a temperature difference ΔT of 2.1 K between the environment and human arm. **d** Measured open-circuit voltage V and resistance of devices R composed of DPF n ($n = 5, 10, 15, 20,$ and 25). Measured **e** V and **f** output power P as a function of loading current I_{load} for the device composed of DPF10 under different ΔT s (10 K and 25 K)

Conclusions

In this work, a rapid and cost-effective wet-spinning method has been employed to prepare PEDOT:PSS fiber bundles, which were doped with DMSO and post-treated by 98% H_2SO_4 . The fiber bundles, consisting of multiple individual PEDOT:PSS fibers, possess low resistance and high tensile strength and stability. The H_2SO_4 post-treatment partially removes excessive PSS units and increases the σ to 4464 S cm^{-1} and power factor up to $80.8 \mu\text{W m}^{-1} \text{ K}^{-2}$, ranking PEDOT:PSS fiber bundles as the best in the current PEDOT:PSS fibers. In addition to this, the fiber bundles exhibit high mechanical properties, and the FTEDs assembled by these fiber bundles show a promising output power of 2.25 nW at a ΔT of 25 K. Our work provides insights into the manufacture of all-organic, flexible, and highly conductive textiles.

Supplementary Information The online version contains supplementary material available at <https://doi.org/10.1007/s42765-024-00374-z>.

Acknowledgements This work was financially supported by the National Natural Science Foundation of China (No. 52272040), the State Key Laboratory of Materials-Oriented Chemical Engineering program (SKL-MCE-23A04), and the Jiangsu Specially Appointed Professor Program. ZGC thanks the financial support from the Australian Research Council, HBIS-UQ Innovation Centre for Sustainable Steel project, and QUT Capacity Building Professor Program. This work was enabled by the use of the Central Analytical Research Facility hosted by the Institute for Future Environments at QUT.

Funding Open Access funding enabled and organized by CAUL and its Member Institutions.

Declarations

Conflict of Interest The authors declare that they have no known competing financial interests or personal relationships that could have appeared to influence the work reported in this paper.

Open Access This article is licensed under a Creative Commons Attribution 4.0 International License, which permits use, sharing, adaptation, distribution and reproduction in any medium or format, as long as you give appropriate credit to the original author(s) and the source, provide a link to the Creative Commons licence, and indicate

if changes were made. The images or other third party material in this article are included in the article's Creative Commons licence, unless indicated otherwise in a credit line to the material. If material is not included in the article's Creative Commons licence and your intended use is not permitted by statutory regulation or exceeds the permitted use, you will need to obtain permission directly from the copyright holder. To view a copy of this licence, visit <http://creativecommons.org/licenses/by/4.0/>.

References

- Cao T, Shi X-L, Chen Z-G. Advances in the design and assembly of flexible thermoelectric device. *Prog Mater Sci.* **2023**;131: 101003.
- Jiang B, Yu Y, Cui J, Liu X, Xie L, Liao J, Zhang Q, Huang Y, Ning S, Jia B, Zhu B, Bai S, Chen L, Pennycook Stephen J, He J. High-entropy-stabilized chalcogenides with high thermoelectric performance. *Science.* **2021**;371:830–4.
- Sarkar D, Samanta M, Ghosh T, Dolui K, Das S, Saurabh K, Sanyal D, Biswas K. All-scale hierarchical nanostructures and superior valence band convergence lead to ultra-high thermoelectric performance in cubic GeTe. *Energy Environ Sci.* **2022**;15:4625–35.
- Yang Q, Yang S, Qiu P, Peng L, Wei T-R, Zhang Z, Shi X, Chen L. Flexible thermoelectrics based on ductile semiconductors. *Science.* **2022**;377:854–8.
- Zheng Z-H, Shi X-L, Ao D-W, Liu W-D, Li M, Kou L-Z, Chen Y-X, Li F, Wei M, Liang G-X, Fan P, Lu G-Q, Chen Z-G. Harvesting waste heat with flexible Bi₂Te₃ thermoelectric thin film. *Nat Sustain.* **2023**;6:180–91.
- Xu S, Shi X-L, Dargusch M, Di C, Zou J, Chen Z-G. Conducting polymer-based flexible thermoelectric materials and devices: from mechanisms to applications. *Prog Mater Sci.* **2021**;121: 100840.
- Zhang L, Shi X-L, Yang Y-L, Chen Z-G. Flexible thermoelectric materials and devices: from materials to applications. *Mater Today.* **2021**;46:62–108.
- Xu H, Guo Y, Wu B, Hou C, Zhang Q, Li Y, Wang H. Highly integrable thermoelectric fiber. *ACS Appl Mater Interfaces.* **2020**;12:33297–304.
- Liu J, Zhu Z, Zhou W, Liu P, Liu G, Xu J, Jiang Q, Jiang F. Flexible metal-free hybrid hydrogel thermoelectric fibers. *J Mater Sci.* **2020**;55:8376–87.
- Wu T, Shi X-L, Liu W-D, Sun S, Liu Q, Chen Z-G. Dual post-treatments boost thermoelectric performance of PEDOT:PSS films and their devices. *Macromol Mater Eng.* **2022**;307:2200411.
- Xu S, Hong M, Shi X-L, Wang Y, Ge L, Bai Y, Wang L, Dargusch M, Zou J, Chen Z-G. High-performance PEDOT:PSS flexible thermoelectric materials and their devices by triple post-treatments. *Chem Mater.* **2019**;31:5238–44.
- Zhou J, Anjum DH, Chen L, Xu X, Ventura IA, Jiang L, Lubineau G. The temperature-dependent microstructure of PEDOT/PSS films: insights from morphological, mechanical and electrical analyses. *J Mater Chem C.* **2014**;2:9903–10.
- Stöcker T, Köhler A, Moos R. Why does the electrical conductivity in PEDOT:PSS decrease with PSS content? A study combining thermoelectric measurements with impedance spectroscopy. *J Polym Sci Pol Phys.* **2012**;50:976–83.
- Culebras M, Gómez CM, Cantarero A. Enhanced thermoelectric performance of PEDOT with different counter-ions optimized by chemical reduction. *J Mater Chem A.* **2014**;2:10109–15.
- Shin S, Roh JW, Kim H-S, Chen R. Role of surfactant on thermoelectric behaviors of organic–inorganic composites. *J Appl Phys.* **2018**;123: 205106.
- Bharti M, Singh A, Samanta S, Aswal DK. Conductive polymers for thermoelectric power generation. *Prog Mater Sci.* **2018**;93:270–310.
- Park T, Park C, Kim B, Shin H, Kim E. Flexible PEDOT electrodes with large thermoelectric power factors to generate electricity by the touch of fingertips. *Energy Environ Sci.* **2013**;6:788–92.
- Komatsu N, Ichinose Y, Dewey OS, Taylor LW, Trafford MA, Yomogida Y, Wehmeyer G, Pasquali M, Yanagi K, Kono J. Macroscopic weavable fibers of carbon nanotubes with giant thermoelectric power factor. *Nat Commun.* **2021**;12:4931.
- Shi X-L, Chen W-Y, Zhang T, Zou J, Chen Z-G. Fiber-based thermoelectrics for solid, portable, and wearable electronics. *Energy Environ Sci.* **2021**;14:729–64.
- Chen W-Y, Shi X-L, Zou J, Chen Z-G. Wearable fiber-based thermoelectrics from materials to applications. *Nano Energy.* **2020**;81: 105684.
- Liu L, Chen J, Liang L, Deng L, Chen G. A PEDOT:PSS thermoelectric fiber generator. *Nano Energy.* **2022**;102: 107678.
- Kim Y, Lund A, Noh H, Hofmann AI, Craighero M, Darabi S, Zokaei S, Park JI, Yoon M-H, Müller C. Robust PEDOT:PSS wet-spun fibers for thermoelectric textiles. *Macromol Mater Eng.* **2020**;305:1900749.
- Xu C, Yang S, Li P, Wang H, Li H, Liu Z. Wet-spun PEDOT:PSS/CNT composite fibers for wearable thermoelectric energy harvesting. *Compos Commun.* **2022**;32: 101179.
- Wen N, Fan Z, Yang S, Zhao Y, Cong T, Xu S, Zhang H, Wang J, Huang H, Li C, Pan L. Highly conductive, ultra-flexible and continuously processable PEDOT:PSS fibers with high thermoelectric properties for wearable energy harvesting. *Nano Energy.* **2020**;78: 105361.
- Yildirim E, Wu G, Yong X, Tan TL, Zhu Q, Xu J, Ouyang J, Wang J-S, Yang S-W. A theoretical mechanistic study on electrical conductivity enhancement of DMSO treated PEDOT:PSS. *J Mater Chem C.* **2018**;6:5122–31.
- Ouyang J, Xu Q, Chu C-W, Yang Y, Li G, Shinar J. On the mechanism of conductivity enhancement in poly(3,4-ethylenedioxythiophene):poly(styrene sulfonate) film through solvent treatment. *Polymer.* **2004**;45:8443–50.
- Cao T, Shi X-L, Zou J, Chen Z-G. Advances in conducting polymer-based thermoelectric materials and devices. *Microstructures.* **2021**;1:2021007.
- Pan Y, Song Y, Jiang Q, Jia Y, Liu P, Song H, Liu G. Solvent treatment of wet-spinning PEDOT:PSS fiber towards wearable thermoelectric energy harvesting. *Synth Met.* **2022**;283: 116969.
- Ge R, Dong X, Sun L, Hu L, Liu T, Zeng W, Luo B, Jiang X, Jiang Y, Zhou Y. Meters-long, sewable, wearable conductive polymer wires for thermoelectric applications. *J Mater Chem C.* **2020**;8:1571–6.
- Sarabia-Riquelme R, Shahi M, Brill JW, Weisenberger MC. Effect of drawing on the electrical, thermoelectrical, and mechanical properties of wet-spun PEDOT:PSS fibers. *ACS Appl Polym Mater.* **2019**;1:2157–67.
- Liu J, Jia Y, Jiang Q, Jiang F, Li C, Wang X, Liu P, Liu P, Hu F, Du Y, Xu J. Highly conductive hydrogel polymer fibers toward promising wearable thermoelectric energy harvesting. *ACS Appl Mater Interfaces.* **2018**;10:44033–40.
- Wen N, Fan Z, Yang S, Zhao Y, Li C, Cong T, Huang H, Zhang J, Guan X, Pan L. High-performance stretchable thermoelectric fibers for wearable electronics. *Chem Eng J.* **2021**;426: 130816.
- Liu Y, Liu P, Jiang Q, Jiang F, Liu J, Liu G, Liu C, Du Y, Xu J. Organic/inorganic hybrid for flexible thermoelectric fibers. *Chem Eng J.* **2021**;405: 126510.

34. Okuzaki H, Harashina Y, Yan H. Highly conductive PEDOT/PSS microfibers fabricated by wet-spinning and dip-treatment in ethylene glycol. *Eur Polym J.* **2009**;45:256–61.
35. Jalili R, Razal JM, Wallace GG. Exploiting high quality PEDOT:PSS–SWNT composite formulations for wet-spinning multifunctional fibers. *J Mater Chem.* **2012**;22:25174–82.
36. Xu T, Ji W, Wang X, Zhang Y, Zeng H, Mao L, Zhang M. Support-free PEDOT:PSS fibers as multifunctional microelectrodes for *in vivo* neural recording and modulation. *Angew Chem Int Ed.* **2022**;61: e202115074.
37. He X, Gu J, Hao Y, Zheng M, Wang L, Yu J, Qin X. Continuous manufacture of stretchable and integratable thermoelectric nanofiber yarn for human body energy harvesting and self-powered motion detection. *Chem Eng J.* **2022**;450: 137937.
38. Feng D, Wang P, Wang M, Zhu C, Gao Q, Shen M. A facile route toward continuous wet-spinning of PEDOT: PSS fibers with enhanced strength and electroconductivity. *Fiber Polym.* **2021**;22:1491–5.
39. Sarabia-Riquelme R, Andrews R, Anthony JE, Weisenberger MC. Highly conductive wet-spun PEDOT:PSS fibers for applications in electronic textiles. *J Mater Chem C.* **2020**;8:11618–30.
40. Meng C, Qian Y, He J, Dong X. Wet-spinning fabrication of multi-walled carbon nanotubes reinforced poly(3,4-ethylenedioxythiophene)-poly(styrenesulfonate) hybrid fibers for high-performance fiber-shaped supercapacitor. *J Mater Sci-Mater El.* **2020**;31:19293–308.
41. Liu G, Jiang F, Liu J, Liu C, Xu J, Jiang Q, Zheng N, Nie G, Liu P. Solvent treatment inducing ultralong cycle stability poly(3,4-ethylenedioxythiophene):poly(styrenesulfonic acid) fibers as binding-free electrodes for supercapacitors. *Int J Energy Res.* **2020**;44:5856–65.
42. Gao Q, Wang M, Kang X, Zhu C, Ge M. Continuous wet-spinning of flexible and water-stable conductive PEDOT: PSS/PVA composite fibers for wearable sensors. *Compos Commun.* **2020**;17:134–40.
43. Zhang J, Seyedin S, Qin S, Lynch PA, Wang Z, Yang W, Wang X, Razal Joselito M. Fast and scalable wet-spinning of highly conductive PEDOT:PSS fibers enables versatile applications. *J Mater Chem A.* **2019**;7:6401–10.
44. Wang X-Y, Feng G-Y, M-J Li, Ge M-Q. Effect of PEDOT:PSS content on structure and properties of PEDOT:PSS/poly(vinyl alcohol) composite fiber. *Polym Bull.* **2019**;76:2097–111.
45. Tian G, Zhou J, Xin Y, Tao R, Jin G, Lubineau G. Copolymer-enabled stretchable conductive polymer fibers. *Polymer.* **2019**;177:189–95.
46. Reid DO, Smith RE, Garcia-Torres J, Watts JF, Crean C. Solvent treatment of wet-spun PEDOT: PSS fibers for fiber-based wearable pH sensing. *Sensors.* **2019**;19:4213.
47. Kim Y, Lim T, Kim C-H, Yeo CS, Seo K, Kim S-M, Kim J, Park SY, Ju S, Yoon M-H. Organic electrochemical transistor-based channel dimension-independent single-strand wearable sweat sensors. *NPG Asia Mater.* **2018**;10:1086–95.
48. Wang X, Feng G-Y, Ge M-Q. Influence of ethylene glycol vapor annealing on structure and property of wet-spun PVA/PEDOT:PSS blend fiber. *J Mater Sci.* **2017**;52:6917–27.
49. Zhou J, Li EQ, Li R, Xu X, Ventura IA, Moussawi A, Anjum DH, Hedhili MN, Smilgies D-M, Lubineau G, Thoroddsen ST. Semi-metallic, strong and stretchable wet-spun conjugated polymer microfibers. *J Mater Chem C.* **2015**;3:2528–38.
50. Wang X, Ge M-Q, Feng G-Y. The effects of DMSO on structure and properties of PVA/PEDOT:PSS blended fiber. *Fiber Polym.* **2015**;16:2578–85.
51. Li X, Liu Y, Shi Z, Li C, Chen G. Influence of draw ratio on the structure and properties of PEDOT-PSS/PAN composite conductive fibers. *RSC Adv.* **2014**;4:40385–9.
52. Jalili R, Razal JM, Wallace GG. Wet-spinning of PEDOT:PSS/functionalized-SWNTs composite: a facile route toward production of strong and highly conducting multifunctional fibers. *Sci Rep.* **2013**;3:3438.
53. Jalili R, Razal JM, Innis PC, Wallace GG. One-step wet-spinning process of poly(3,4-ethylenedioxythiophene):poly(styrenesulfonate) fibers and the origin of higher electrical conductivity. *Adv Funct Mater.* **2011**;21:3363–70.
54. Kadlec L, Kwon YW, Haller C, Park CM, Didoszak JM. Tensile and cyclic loading of fiber bundles. *Multiscale Multidiscip Model Exp Des.* **2021**;4:245–57.